PHOTOSYNTHETICA
International Journal for Photosynthesis Research

DOI 10.32615/ps.2026.033 PHOTOSYNTHETICA 64 (3): 223-231, 2026

Determination of chlorophyll and carotenoid content in Mediterranean riparian forest species using visible spectroscopy

M. MARTÍNEZ MENA[*,+], M.D.L. SOTO ROSALES[**], and D. GARCÍA DE JALÓN[*]

Hydrobiology Group, Department of Systems and Natural Resources, Higher Technical School of Forestry, Forest and Natural Environment, Polytechnic University of Madrid, University City, 28040 Madrid, Spain[*]
National Polytechnic Institute, Higher School of Economics, Plan de Agua Prieta 66, Plutarco Elías Calles, Miguel Hidalgo, 11350 Mexico City, Mexico[**]

Abstract

Leaf-level optical measurements are essential for monitoring Mediterranean riparian forests. This study used visible spectroscopy (400–750 nm) to determine and quantify leaf pigments in five species: *Salix salviifolia*, *Fraxinus angustifolia*, *Alnus glutinosa*, *Populus nigra*, and *Prunus avium*. We followed Hansmann's method for sample processing and quantified chlorophyll using Arnon's equation. We collected samples from sun-exposed leaves in spring under standardized conditions. Results indicated that *Alnus glutinosa* and *Populus nigra* exhibited the highest chlorophyll *a* concentrations [1.35 and 1.29 mg g^{-1} (FM)], followed by *Fraxinus angustifolia* [1.17 mg g^{-1}(FM)], *Salix salviifolia* [0.61 mg g^{-1}(FM)], and *Prunus avium* [0.25 mg g^{-1}(FM)]. The chlorophyll *a*/*b* ratio exceeded 2.0 in most species, peaking in *Salix salviifolia* (2.90). These findings reveal significant functional differences in pigment composition, confirming the utility of this method for monitoring the physiological status of the vegetation in the Manzanares River, Spain.

Keywords: chlorophyll *a*; chlorophyll *a*/*b* ratio; Manzanares River; riparian forest; visible spectroscopy.

Introduction

Riparian vegetation is among the most dynamic yet threatened terrestrial ecosystems (Stella *et al.* 2019, Camarero *et al.* 2025). These ecosystems play a fundamental role in mitigating flood risk; they not only enhance ecological connectivity but also modulate flow velocity, stabilize riverbanks, and attenuate peak floods (Riis *et al.* 2020, Díaz-Redondo *et al.* 2022). Although riparian vegetation may appear as isolated or fragmented islands, it often forms continuous corridors along river channels (Del Tánago *et al.* 2021). During floods, this vegetation acts as a hydraulic shock absorber, reducing the risk of flooding (Sabo *et al.* 2005, Yan *et al.* 2025).

Riparian vegetation is increasingly threatened by anthropogenic pressures, including land use change, water diversion, altered flow regimes, forest fires, invasive species, and droughts, which have reduced these ecosystems to narrow strips or, in some cases, eliminated them (Casotti *et al.* 2015, Gran *et al.* 2015, Havrdová *et al.* 2023). Growth depends on soil water availability, flood regimes, sediment types, and light

Highlights

- Spectral characterization of five Mediterranean riparian forest species was performed
- Chlorophyll *a* showed λ_{max} at 432–433 and 663–664 nm
- Chlorophyll *b* exhibited absorption maxima near 454 and 645–647 nm, overlapping with carotenoids in the blue region

Received 20 March 2026
Accepted 21 September 2026
Published online 13 October 2026

[+]Corresponding author
e-mail: guadalupe.martinez.mena@alumnos.upm.es

Abbreviations: A – absorbance; A_{645} – absorbance at 645 nm; A_{663} – absorbance at 663 nm; *ANOVA* – analysis of variance; Chl – chlorophyll; FM – fresh mass; SE – standard error; UV-Vis – ultraviolet-visible; v/v – volume per volume.
Acknowledgements: The authors thank the head of the Laboratory of Coordination and Organometallic Chemistry at the Universidad Complutense de Madrid for lending the equipment for the experiments.
Conflict of interest: The authors declare that they have no conflict of interest.

(Gran *et al*. 2015, Del Tánago *et al*. 2021). Its presence within fluvial systems improves water quality and protects riverbanks. Consequently, restoration and conservation projects (Del Tánago *et al*. 2021, Díaz-Alba *et al*. 2023) must account for long-term interactions between the river and vegetation, incorporating hydrological and climatic variability (Rodríguez-González *et al.* 2010, Gurnell *et al.* 2020, Deng *et al.* 2024, Camarero *et al*. 2025).

Optical remote sensing, using optical reflectance and absorbance sensors (Abdullah *et al.* 2018, Pérez-Patricio *et al.* 2018, Barbosa *et al*. 2024, Kior *et al*. 2024), is becoming a viable alternative for identifying plant senescence stages (Casotti *et al*. 2015, Bednaříková *et al*. 2023, Du *et al.* 2025). UV–Vis spectroscopy in plants provides quantitative information on pigment composition, electronic transitions, and molecular structures (Houborg *et al*. 2015, Barbosa *et al*. 2024, Alaboodi *et al*. 2025, Gao *et al.* 2025).

Chlorophyll is a green pigment whose primary function is to absorb sunlight in the blue and red wavelengths; this largely determines photosynthetic capacity, as well as plant growth and development (Chen and Blankenship 2011, Mulero *et al*. 2022, Gong *et al*. 2023).

Several types of chlorophyll exist (*a*, *b*, *c*, *d*, and *f*), all of them green. Their structural differences result in variations in their absorption spectra and, consequently, in their specific green hues: chlorophyll *a* is blue-green, chlorophyll *b* is bright green, chlorophyll *c* is yellow-green, chlorophyll *d* is forest/bright green, and chlorophyll *f* is emerald green (Chen *et al*. 2010, Qiu *et al.* 2019). Chlorophyll *a* primarily absorbs violet and orange light (with absorption maxima at 372 and 642 nm). Chlorophyll *b* mainly absorbs blue and yellow light, with absorption maxima at 392 and 626 nm. Both pigments also absorb other wavelengths with lower intensity. However, neither absorbs green light efficiently; thus, leaves appear green because this light is reflected into our eyes instead of being absorbed (Milne *et al*. 2015).

Materials and methods

Study area: The sampling site was located along a restored section of the Manzanares River (Madrid, Spain), approximately 800 m downstream of the El Pardo dam, near the Mingorrubio pedestrian bridge (Fig. 1*D*). The site is situated within a restricted military zone; the area was selected as part of an ecological restoration project aimed at recovering natural river dynamics.

In 2024, the highest monthly precipitation was recorded in November (60.8 ± 4.2 mm), reflecting significant seasonal rainfall variability. The highest average temperature occurred in July (31.6 ± 1.8°C), while during the spring season (March–May), the average temperature was (21.2 ± 2.5°C), indicating a stable thermal transition with moderate seasonal deviation (AEMET 2024).

Changes in rainfall and temperature can reduce water availability for riparian species, especially during sensitive stages such as flowering (Martínez-Fernández *et al.* 2018, Del Tánago *et al*. 2021). Therefore, understanding the interactions between climate variability and forest phenology is essential for assessing their ecological and physiological impacts.

Selection of riparian forest species: For this study, *Salix salviifolia* Brot., *Alnus glutinosa* (L.) Gaertn., *Populus nigra* L., *Fraxinus angustifolia* Vahl, and *Prunus avium* (L.) were selected, as they are the most common species in the studied section of the Manzanares River.

Salix salviifolia is a small deciduous tree belonging to the Salicaceae family and the genus *Salix*, reaching

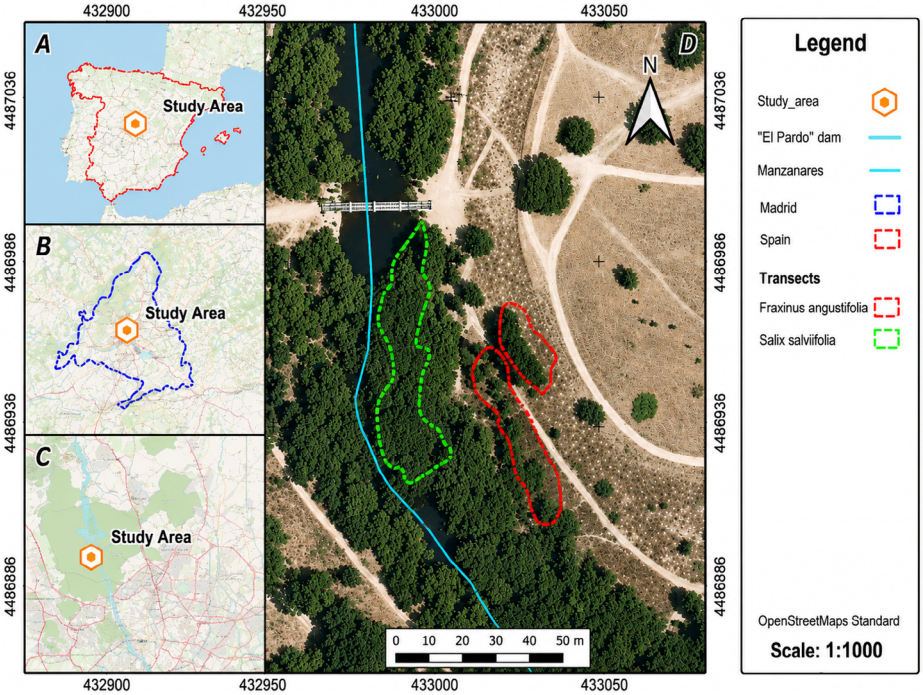


Fig. 1. Study area: (*A*) map of Spain; (*B*) location of the Community of Madrid; (*C*) Manzanares River downstream of El Pardo reservoir; (*D*) study transects with *Fraxinus angustifolia* highlighted *in red* and *Salix salviifolia in green*; the basemap corresponds to an orthophoto from the Spanish National Aerial Orthophotography Program.

a maximum height of approximately 6 m. Its leaves are simple and oval-shaped, measuring 5 to 10 cm in length, with a long, narrow, pointed apex and a dark grayish green color (López González 2006). This species is distributed along the upper and middle reaches of the river, particularly in areas in direct contact with the water-contact zone (González *et al*. 2018, Del Tánago *et al*. 2021). This species is native to the Iberian Peninsula; it is characterized by high water requirements and significant flood tolerance (Lozanovska *et al*. 2020).

Fraxinus angustifolia is a deciduous tree in the Oleaceae family and the genus *Fraxinus*, typically reaching 10–15 m. Its compound leaves have an odd number of lanceolate leaflets with toothed margins, 5 to 13 cm long; they are green (Castroviejo 2020). This species is native to the Iberian Peninsula (López González 2006). This species is characteristic of alluvial plains and is well-adapted to summer droughts (Camarero *et al*. 2023).

Alnus glutinosa is a deciduous tree in the Betulaceae family and the genus *Alnus*, of medium height between 20–25 m, with very fast growth when young. Its leaves are characterized by a rounded shape, 4–10 cm in length and 5–7 cm in width, with serrated edges, dark green on the upper side and paler on the underside (López González 2006, Castroviejo 2020).

Populus nigra is a deciduous tree of the Salicaceae family and the genus *Populus*, growing up to 30 m in height with an annual growth rate of approximately 1 m per year; it typically does not exceed a lifespan of 100 years. Its leaves have a rhomboidal silhouette, are 2–6 cm long, and are intensely green; it is a fast-growing species (Castroviejo 2020). Distributed across much of Europe, it grows in groves and riparian areas with high light availability (López González 2006).

Prunus avium is a deciduous tree from the Rosaceae family and the genus *Prunus*; it is distinguished by its showy clusters of 15–30 flowers, reaching heights of 15–25 m. Its leaves are lanceolate and elliptical, green in color and, when young, have a reddish tinge, measuring 6–15 cm in length (López González 2006, Castroviejo 2020).

Instrumentation: Absorbance spectra were recorded using a *Cary-5G/5000* ultraviolet, visible, and near-infrared (UV/Vis/NIR) dual-beam spectrophotometer (*Agilent Technologies*) equipped with two quartz cuvettes. Although the instrument provides a spectral range of 360–1,200 nm, measurements were specifically performed within the 400–750 nm range. The system is fitted with a *PbSmart* detector, ensuring high photometric accuracy across both the visible and near-infrared (NIR) regions. Data acquisition and processing were conducted using *Cary WinUV* software.

Baseline calibration and measurement protocol: The spectrophotometer was calibrated using two quartz cuvettes with a 1-cm optical path length. One cuvette containing the solvent [90% (v/v) acetone/water] served as the blank (reference signal), while the other cuvette contained the green extract with no turbidity or suspended particles. This reference signal was used as a baseline for all subsequent spectral measurements.

Leaf sampling: Sampling was carried out under stable weather conditions during the spring in 2024, characterized by clear skies, windless conditions, and cloudless conditions. Leaf collection was performed between 7:00 and 9:00 h to minimize the effects of diurnal variation on leaf water content and photosynthetic activity, thereby preventing alterations in spectral measurements. All samples were collected on the same day to reduce environmental and phenological variability, coinciding with the onset of the early spring growth period.

From each individual, ten leaves were harvested using pruning shears to ensure minimal damage to the surrounding foliage. Only physiologically mature, healthy, and fully expanded leaves were selected. In addition to interspecific differences, variations in color intensity were observed in specific leaf regions, such as the midrib and the apex, where light absorption is typically greater.

Sample preservation: Leaf samples were placed in labeled paper bags and transported in a portable cooler with ice packs at approximately 4°C. Throughout sample handling, the leaves were kept shaded, and samples were transported to the laboratory as quickly as possible to maintain their biochemical and physical properties.

Experimental procedure: For each sample, 0.4 g of fresh leaf tissue was weighed after being cleaned and finely chopped. The leaf material was then suspended in 5 mL of a 90% acetone–water solution (v/v), which served as the solvent for pigment extraction. The leaf sample mixtures were kept in the dark at 2°C for 48 h until a homogeneous green solution without turbidity was obtained, suitable for spectroscopic analysis. As previously mentioned, the experimental procedure was carried out using plant samples collected from the selected species. The experimental procedure was applied to 13 samples for each of the forest species under study.

Spectrophotometric method: The Hansmann (Ríos Cortés *et al*. 2017) spectrophotometric method was used to identify the characteristic absorption peaks of the photosynthetic pigments. Although absorbance values were recorded continuously across the 400–750 nm range, absorbance values at 645 and 663 nm were selected for further analysis. Measurements at these two wavelengths resulted in a total of 130 spectral readings.

Chlorophyll quantification: Sample concentrations were adjusted to ensure that all measurements adhered to the Beer–Lambert law and remained within the spectrophotometer's linear dynamic range. Concentrations were calculated using the equations proposed by Arnon (1949), based on absorbance readings at 645 and 663 nm expressed in mg L^{-1} as follows:

$$\text{Chl } a = 12.7A_{663} - 2.69A_{645} \quad (1)$$

$$\text{Chl } b = 22.9A_{645} - 4.68A_{663} \quad (2)$$

$$\text{Chl total} = 20.2A_{645} + 8.02A_{663} \quad (3)$$

$$C\ (x+c) = (1{,}000A_{470} - 2.27Ca - 81.4Cb)/227 \quad (4)$$

where A_{663}, A_{645}, and A_{470} represent the absorbance values measured at the respective wavelengths, C (x+c) is the concentration of carotenoids, and Ca and Cb are the concentrations of Chl.

Chlorophyll concentration: To calculate the chlorophyll concentration relative to leaf fresh mass (FM), expressed in mg g^{-1}(FM), the chlorophyll concentration was calculated using the following equation:

$$Chl_{FW} = (C_e \times V_e \times DF)/W \quad (5)$$

where: C_e represents the chlorophyll concentration expressed in mg L^{-1}, calculated using the Arnon equation; V_e is the total volume of solvent used for extraction, expressed in mL; W is the leaf sample fresh mass expressed in g; DF is the dilution factor (1:10). This calculation enables a standardized comparison of chlorophyll content across species and treatments, independent of the extraction volume.

Determination of total carotenoids: In the extract of plant material, A_{470} (the carotenoid region) is determined as the sum of specific absorbances for Chl *a*, Chl *b*, and total carotenoids:

$$A_{470} = A(x+c)_{470} + A(a)_{470} + A(b)_{470} \quad (6)$$

The concentration of carotenoids C (x+c) is:

$$C(x+c) = \frac{A_{(a)470} - (\alpha_{(a)470} \times Ca) - (\alpha_{(b)470} \times Cb)}{\alpha_{(x+c)470}} \quad (7)$$

where α is the specific absorbance coefficient and Ca and Cb are the concentrations of Chl.

Statistical analysis: An analysis of variance (*ANOVA*) was applied to determine if statistically significant differences existed in chlorophyll concentrations among the five forest species. Absorbance values at 645 and 663 nm were used as the primary response variables.

Results

Chlorophyll quantification: Concentrations of chlorophyll *a* and chlorophyll *b* for the five forest species are summarized in Table 1. These results, expressed in mg L^{-1} and including the standard error (± SE), provide the chlorophyll content for each species while indicating the variability and analytical precision among samples.

Visible spectral absorption profile: The absorption profiles (*black line*) presented in Fig. 2 for *Fraxinus angustifolia*, *Salix salviifolia*, *Alnus glutinosa*, *Populus nigra*, and *Prunus avium* highlight the primary absorption features associated with photosynthetic pigments, specifically Chl *a* and Chl *b*.

Fraxinus angustifolia exhibited two principal absorption maxima. The first occurred at approximately 433 nm and was assigned to the Soret (B) band of Chl *a*. In contrast, the second maximum, observed at 663 nm, corresponded to the Q_y band of Chl *a*. A secondary absorption feature near 454 nm was associated with the overlapping contribution of Chl *b* and carotenoids. Absorbance decreased markedly between approximately 500 and 560 nm and approached zero beyond 700 nm.

Salix salviifolia showed two absorption maxima at 433 and 663 nm, corresponding to the Soret (B) and Q_y bands of Chl *a*, respectively. A secondary absorption band near 454 nm was attributed to overlapping absorption by Chl *b* and carotenoids. Absorbance was low in the green–yellow region, particularly between approximately 500–580 nm, and declined rapidly after the red absorption maximum.

Populus nigra showed two principal absorption maxima: one in the blue region at approximately 432 nm and another in the red region at approximately 663–664 nm. These values were assigned to the Soret (B) band and Q_y bands of Chl *a*, respectively. A secondary band near 454 nm indicated overlapping contributions from Chl *b* and carotenoids. Absorbance decreased substantially between approximately 500–580 nm and reached values close to zero beyond 700 nm.

Alnus glutinosa exhibited a prominent absorption maximum in the blue region (432–433 nm) and a second maximum in the red region (663–664 nm), corresponding to the Soret (B) and Q_y bands of Chl *a*. The absorption feature near 454 nm was attributed to overlapping contributions from Chl *b* and carotenoids. Low absorbance values were observed throughout most of the 500–600 nm region, followed by a marked decline beyond the red maximum.

Prunus avium exhibited three relevant absorption maxima at approximately 412, 432, and 454 nm in the blue region, together with a distinct red maximum at approximately 664 nm. The maximum at 432 nm

Table 1. Calculation of the concentrations of chlorophyll *a* (Chl *a*) and chlorophyll *b* (Chl *b*) and total chlorophyll expressed in mg L^{-1}, determined by the Arnon equation.

Species	Chl *a* [mg L^{-1}]	Chl *b* [mg L^{-1}]	Chl (*a*+*b*) [mg L^{-1}]
Fraxinus angustifolia	9.38 ± 0.38	3.73 ± 0.12	13.11 ± 0.51
Salix salviifolia	4.90 ± 0.44	1.64 ± 0.13	6.55 ± 0.58
Alnus glutinosa	10.80 ± 0.82	4.05 ± 0.25	14.85 ± 1.08
Populus nigra	10.29 ± 0.57	4.29 ± 0.19	14.59 ± 0.76
Prunus avium	2.00 ± 0.14	1.01 ± 0.02	3.02 ± 0.15

was assigned to the Soret (B) band of Chl *a*, whereas the feature at 454 nm was associated with overlapping absorption by Chl *b* and carotenoids. The red maximum at 664 nm corresponded to the Q_y band of Chl *b*. Absorbance decreased markedly between approximately 500–600 nm.

The UV–Vis spectra of the studied riparian species, *Salix salviifolia*, *Fraxinus angustifolia*, *Prunus avium*, *Alnus glutinosa*, and *Populus nigra* showed the characteristic absorption bands of photosynthetic pigments. In all species, an intense absorption maximum was observed at approximately 432–433 nm. It was assigned to the Soret (B) band of Chl *a*, mainly associated with high-energy ($n\rightarrow\pi^*$) electronic transitions within the conjugated chlorin system. A secondary maximum near 454 nm was also detected and was related to the overlapping contributions of Chl *b* and carotenoids. In the lower-energy red region, a prominent maximum was observed at approximately 663–664 nm, corresponding to the Q_y band of Chl *a* and also arising mainly from ($n\rightarrow\pi^*$) transitions (Taniguchi *et al*. 2021).

On the other hand, ($n\rightarrow\pi^*$) transitions are less photoactive, as they have a lower capacity to absorb light (Newberry and Raines 2017). The ($\sigma\rightarrow\sigma^*$) transitions occur in the far ultraviolet (UV) region, which was outside the measured range.

Spectral characterization and pigment dynamics: The five riparian forest species showed Chl *a* absorption maxima at approximately 432–433 nm in the Soret (B) band and at 663–664 nm in the Q_y band. An overlapping maximum near 454 nm was attributed to Chl *b* and carotenoids, contributing to the spectral signatures of the analyzed extracts.

Chlorophyll concentration: The results of the Chl concentrations for the five riparian forest species are presented in Table 2. *Alnus glutinosa* and *Populus nigra* exhibited the highest total chlorophyll; the values were 1.86 ± 0.14 and 1.84 ± 0.10 mg g^{-1}(FM). These were followed by *Fraxinus angustifolia* [1.64 ± 0.06 mg g^{-1}(FM)]. In contrast, *Salix salviifolia* showed moderate values [1.22 ± 0.11 mg g^{-1}(FM)], while *Prunus avium* showed the lowest pigment content [0.38 ± 0.02 mg g^{-1}(FM)].

Chlorophyll analysis: One-way *ANOVA* revealed that *Alnus glutinosa* and *Populus nigra* showed the highest chlorophyll concentrations, particularly in Chl *a*. *Fraxinus angustifolia* also showed elevated values. *Salix salviifolia* exhibited moderate yet stable concentrations of both Chl *a* and Chl *b*, ranking above *Prunus avium*, which presented the lowest Chl. Marked differences in Chl concentration were observed between the studied species, as shown in Fig. 3.

The one-way *ANOVA* results revealed remarkably high F-statistic values for Chl *a*, *b*, and total chlorophyll (F = 53.474, 82.183, and 44.558, respectively; $p<0.001$ in all cases) using *Origin 2026* software. The values obtained

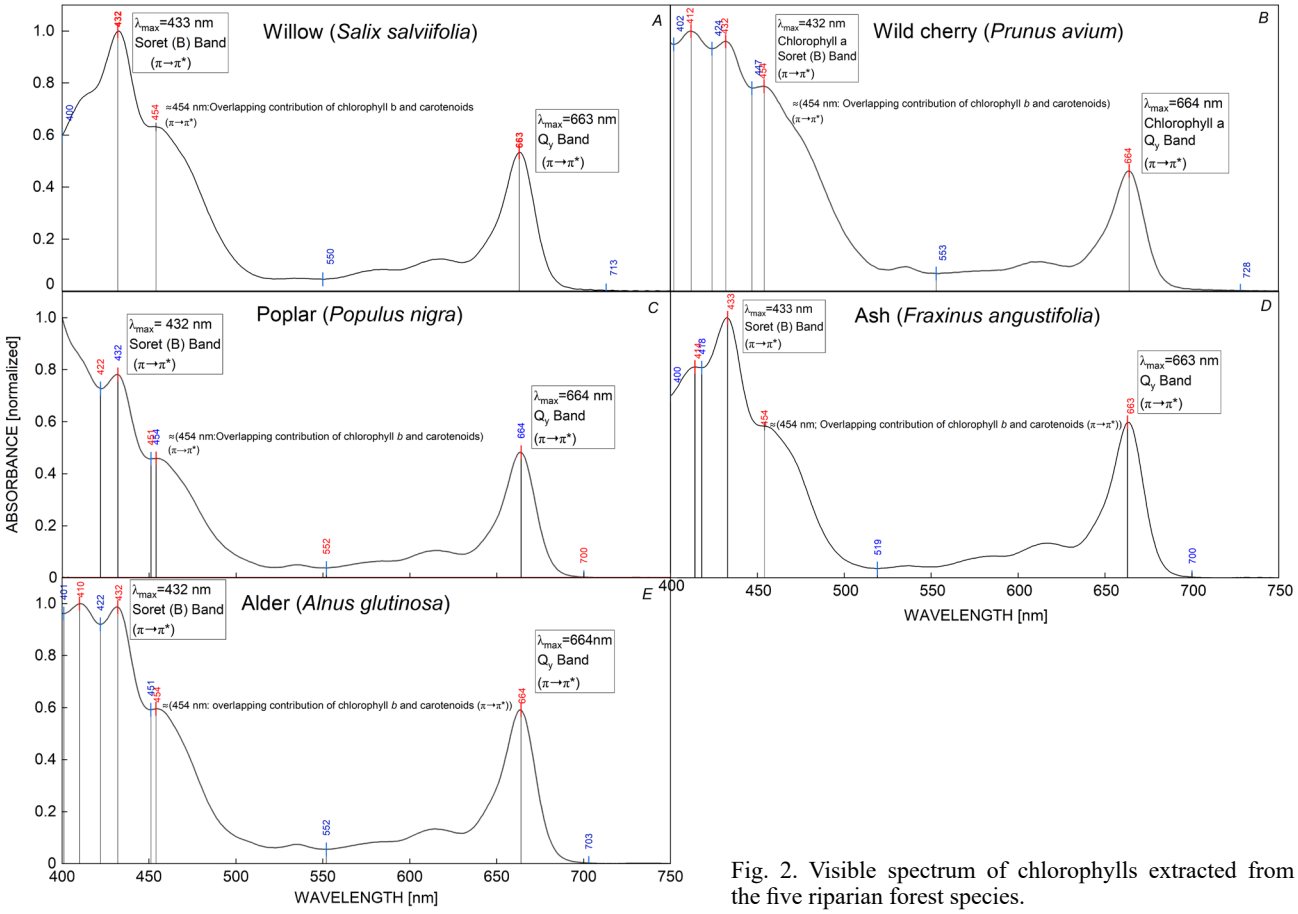


Fig. 2. Visible spectrum of chlorophylls extracted from the five riparian forest species.

Table 2. Contents of chlorophyll a (Chl *a*), chlorophyll b (Chl *b*), total chlorophyll [Chl (*a*+*b*)], and chlorophyll ratio (Chl *a*/*b*) in milligrams per gram of fresh mass [mg g^{-1}(FM)] for the leaves of *Fraxinus angustifolia*, *Salix salviifolia*, *Alnus glutinosa*, *Populus nigra*, and *Prunus avium*.

Species	Chl *a* [mg g^{-1}(FM)]	Chl *b* [mg g^{-1}(FM)]	Chl (*a*+*b*) [mg g^{-1}(FM)]	Chl *a*/*b* ratio
Fraxinus angustifolia	1.17 ± 0.05	0.47 ± 0.02	1.64 ± 0.06	2.49
Salix salviifolia	0.61 ± 0.06	0.21 ± 0.02	0.82 ± 0.07	2.90
Alnus glutinosa	1.35 ± 0.10	0.51 ± 0.03	1.86 ± 0.14	2.65
Populus nigra	1.29 ± 0.07	0.54 ± 0.02	1.84 ± 0.10	2.39
Prunus avium	0.25 ± 0.02	0.13 ± 0.00	0.38 ± 0.02	1.92

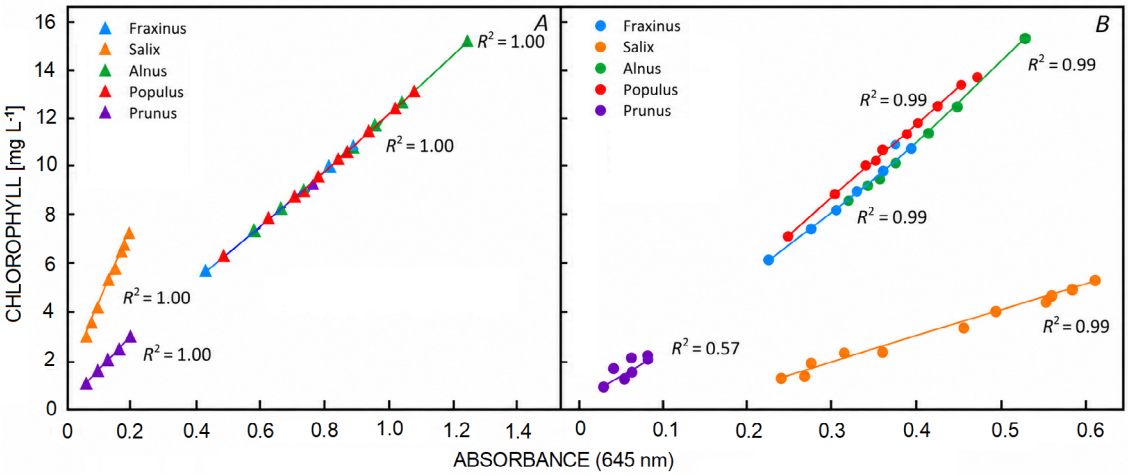


Fig. 3. (*A*) Chlorophyll *a* and (*B*) chlorophyll *b* concentrations present in the extracts of *Fraxinus angustifolia*, *Salix salviifolia*, *Alnus glutinosa*, *Prunus avium*, and *Populus nigra*.

suggest differences in photosynthetic pigment composition between the species. This modulation in pigment composition may reflect physiological adjustments to the light gradients characteristic of the riverbank. As an additional qualitative assessment of the spectral behavior of chlorophylls, the relative absorption curves of Chl *a* and *b* were plotted, revealing crossover points between them. Based on graphical interpolation, the curves were found to intersect at approximately 442.7 nm in the blue region and 650.8 nm in the red region (Fig. 4). Relative absorption ≈ 0.70 at 443 nm in the blue region and ≈ 0.70 at 651 nm in the red region; these wavelengths are commonly used to estimate total chlorophyll.

Discussion

The variations observed in photosynthetic pigments (Croft *et al.* 2017) suggest that the studied species employ divergent ecophysiological strategies to optimize photosynthetic performance, as seen in Table 1. The significantly elevated chlorophyll contents observed in *Alnus glutinosa*, *Populus nigra*, and *Fraxinus angustifolia* suggest high light availability. In these species, allocating more energy to chlorophyll production would facilitate the rapid growth rates characteristic of pioneer riparian species (Sabo *et al.* 2005, Gurnell *et al.* 2020), as seen in Fig. 3. Conversely, the lower chlorophyll concentration in *Prunus avium* could reflect an adaptation to lower solar incidence.

In the riparian vegetation sampling area, the predominant soils are Cambisols developed on clayey silts, sands, gravels, and pebbles, which are characterized by a significant proportion of clays and iron oxides (IUSS Working Group WRB 2015). These soils may favor certain agricultural uses; however, they can be susceptible to erosion, particularly without tree canopy cover or when soil conservation practices are not implemented (Regodón 1970, Cid Rusiñol *et al.* 2023). The province of Madrid has a Mediterranean climate influenced by its relief, particularly the Sierra de Guadarrama. It has hot, dry summers and cooler, wetter winters. The north–south altitudinal gradient produces marked differences in temperature and precipitation, as observed along the Manzanares River basin (Montes *et al.* 1987, Sinclair *et al.* 2024, Santiago and García de Jalón 2026).

In 2024, the Community of Madrid recorded a mean annual precipitation of 475.6 mm, corresponding to 96% of the 1991–2020 reference value, and the year was classified as normal for precipitation. However, precipitation showed marked seasonal variability: April, May, July, and November were classified as very dry, whereas December was extremely dry and the second-driest December in the historical record (AEMET 2024).

The Chl *a*/*b* ratio also varied among species, ranging from 1.92 in *Prunus avium* to 2.90 in *Salix salviifolia*.

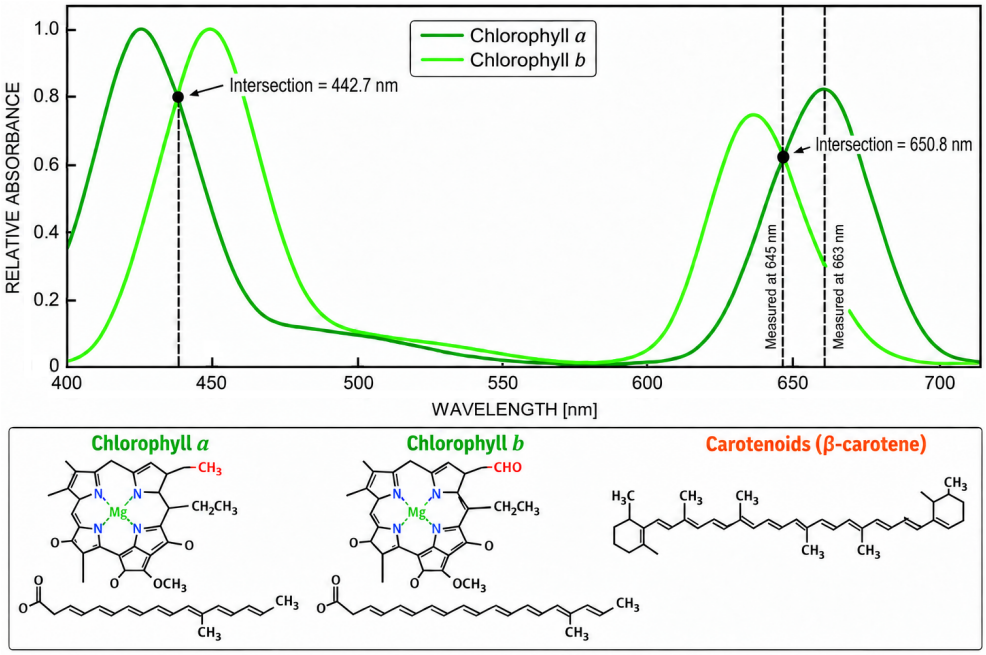


Fig. 4. Schematic absorption bands of chlorophyll *a* and *b* with values and theoretical intersections and molecular structure of chlorophylls *a* and *b* and β-carotene.

Intermediate values were observed in *Alnus glutinosa* (2.65), *Fraxinus angustifolia* (2.49), and *Populus nigra* (2.39), as shown in Table 2. These differences may reflect species-specific variations in composition and organization of photosynthetic pigments under local environmental conditions. Trees in this region are exposed to a Mediterranean climate characterized by hot, dry summers, during which high temperatures coincide with low precipitation availability (Montes *et al.* 1987, AEMET 2024). These conditions may influence vegetation morphology and the functioning of Mediterranean riparian forest and, together with local soil conditions, contribute to the observed variation in the Chl *a*/*b* ratio.

The Chl *a*/*b* ratio can also indicate the relative organization of the light-harvesting antenna (Lichtenthaler and Babani 2022, Zahn *et al.* 2026). The data reveal a clear hierarchy among the species based on their specific light requirements, as seen in Table 2: sun-loving species (*Salix salviifolia* and *Alnus glutinosa*) exhibited the highest ratios. The dominance of Chl *a* is typical for plants growing in open spaces with high light availability. These riparian forest species prioritize processing energy quickly to prevent cell damage from excessive sunlight (Gao *et al.* 2025).

Intermediate species (*Fraxinus angustifolia* and *Populus nigra*) showed balanced values, suggesting high plasticity in adapting to varying light levels within the riparian zone. Shade-adapted species (*Prunus avium*) showed the lowest value in the series. A ratio below 2.0 indicates a proportional increase in Chl *b*, as seen in Table 2. Biologically, this suggests a strategy for surviving in low-light environments, where plants produce more "support pigments" in their antennas to capture the limited light that filters through the taller tree canopy (Zahir *et al.* 2022).

The identification of the crossover point at 650.8 nm and 442.7 nm serves as a critical quality control measure that reinforces the validity of the entire analysis, as shown in Fig. 4. Following the criteria established by Mackinney (1941), this point represents the exact equilibrium where the absorption coefficients of Chl *a* and *b* are identical, a finding later integrated into the standard protocols by Arnon (1949).

Conclusions: The differences observed in the photosynthetic pigments of riparian species may reflect specific responses to light availability and their location along the riverbank. *Populus nigra*, *Alnus glutinosa*, and *Fraxinus angustifolia* exhibited relatively high chlorophyll *a* and *b* contents. All five species showed chlorophyll *a* absorption maxima at 432–433 nm in the Soret (B) band and at 663–664 nm in the Q_y band, as well as an absorption feature near 454 nm attributed to the combined contribution of chlorophyll *b* and carotenoids. Furthermore, the chlorophyll *a* and *b* curves showed a crossover point around 442.7 nm in the blue region and 650.8 nm in the red region, which constitutes an additional useful spectral reference for the characterization and monitoring of riparian forest species in the transect of River Manzanares.

References

Abdullah H., Darvishzadeh R., Skidmore A.K. *et al.*: European spruce bark beetle (*Ips typographus*, L.) green attack affects foliar reflectance and biochemical properties. – Int. J. Appl. Earth Obs. Geoinf. **64**: 199-209, 2018.

AEMET: Spanish State Meteorological Agency: forecasts, advisories, observations, situation report, 2024. *Available at*: https://www.aemet.es/es/datos_abiertos. [In Spanish]

Alaboodi A.S., Kadhim S.A., Hussein A.S.: Ultraviolet-visible spectroscopy, importance, principle, structure and most important applications: a study review. – Int. J. Nov. Res. Phys. Chem. Math. **12**: 53-60, 2025.

Arnon D.I.: Copper enzymes in isolated chloroplasts. Polyphenoloxidase in *Beta vulgaris*. – Plant Physiol. **24**: 1-15, 1949.

Barbosa T.K.M., Fiorio P.R., Calaboni C. *et al.*: Lisianthus (*Eustoma grandiflorum*) leaf degradation analysis in the postharvest by VIS-NIR-SWIR reflectance spectroscopy. – Ciênc. Rural **54**: e20230143, 2024.

Bednaříková M., Gauslaa Y., Solhaug K.A.: Non-invasive monitoring of photosynthetic activity and water content in forest lichens using spectral reflectance data and RGB colors from photographs. – Fungal Ecol. **62**: 101224, 2023.

Camarero J.J., Colangelo M., Rodríguez-González P.M.: Tree growth, wood anatomy and carbon and oxygen isotopes responses to drought in Mediterranean riparian forests. – Forest Ecol. Manag. **529**: 120710, 2023.

Camarero J.J., Gazol A., Fernández-Cortés Á., Colangelo M.: Riparian field elm (*Ulmus minor*) is sensitive to drought, and fast-growing trees are susceptible to Dutch elm disease. – Forest Ecol. Manag. **594**: 122948, 2025.

Casotti C.G., Kiffer Jr W.P., Costa L.C. *et al.*: Assessing the importance of riparian zones conservation for leaf decomposition in streams. – Natur. Conserv. **13**: 178-182, 2015.

Castroviejo S., Aedo C., Cirujano S. *et al.*: [Flora Ibérica: Vascular Plants of the Iberian Peninsula and the Balearic Islands.] Pp. 784. CSIC, Madrid 2020. [In Spanish]

Chen M., Blankenship R.E.: Expanding the solar spectrum used by photosynthesis. – Trends Plant Sci. **16**: 427-431, 2011.

Chen M., Schliep M., Willows R.D. *et al.*: A red-shifted chlorophyll. – Science **329**: 1318-1319, 2010.

Cid Rusiñol M., Sánchez Fayos Calabuig T., Villacañas Beades S.: [Special plan for the protection and improvement of the green infrastructure of the metropolitan forest of Madrid. Lot 1. General Directorate of Strategic Planning.] Ayuntamiento de Madrid, Madrid 2023. *Available at*: https://servpub.madrid.es/VECSV_WBCONSULTA/VerificarCove.do. [In Spanish]

Croft H., Chen J.M., Luo X. *et al.*: Leaf chlorophyll content as a proxy for leaf photosynthetic capacity. – Glob. Change Biol. **23**: 3513-3524, 2017.

Del Tánago M.G., Martínez-Fernández V., Aguiar F.C. *et al.*: Improving river hydromorphological assessment through better integration of riparian vegetation: Scientific evidence and guidelines. – J. Environ. Manage. **292**: 112730, 2021.

Deng X., Greet J., Jones C.S.: Soil moisture influences the root characteristics of a herbaceous riparian plant along a regulated river. – Plant Ecol. **225**: 25-36, 2024.

Díaz-Alba D., Henry A.L., de Jalón D.G. *et al.*: Salix regeneration in fluvial landscapes: Empirical findings based on a systematic review. – Ecol. Eng. **193**: 107010, 2023.

Díaz-Redondo M., Marchamalo M., Morcillo F., King J.J.: Naturalising a heavily modified urban river: Initial habitat evolution in the Manzanares River (Madrid, Spain). – River Res. Appl. **38**: 727-737, 2022.

Du S., Zhao D., Guan L. *et al.*: PROSPECT-DP: A coupled leaf optical properties model for improving leaf spectra simulation in the red-edge domain by excluding the ChlF effect. – Int. J. Appl. Earth Obs. Geoinf. **141**: 104651, 2025.

Gao R.-Y., Zou J.-W., Shi Y.-P. *et al.*: The Q-band energetics and relaxation of chlorophylls *a* and *b* as revealed by visible-to-near infrared time-resolved absorption spectroscopy. – J. Phys. Chem. Lett. **16**: 789-794, 2025.

Gong L., Zhu C., Luo Y., Fu X.: Spectral reflectance reconstruction from red-green-blue (RGB) images for chlorophyll content detection. – Appl. Spectrosc. **77**: 200-209, 2023.

González E., Martínez-Fernández V., Shafroth P.B. *et al.*: Regeneration of *Salicaceae* riparian forests in the Northern Hemisphere: a new framework and management tool. – J. Environ. Manage. **218**: 374-387, 2018.

Gran K.B., Tal M., Wartman E.D.: Co-evolution of riparian vegetation and channel dynamics in an aggrading braided river system, Mount Pinatubo, Philippines. – Earth Surf. Proc. Land. **40**: 1101-1115, 2015.

Gurnell A.M., Scott S.J., England J. *et al.*: Assessing river condition: A multiscale approach designed for operational application in the context of biodiversity net gain. – River Res. Appl. **36**: 1559-1578, 2020.

Havrdová A., Douda J., Doudová J.: Threats, biodiversity drivers and restoration in temperate floodplain forests related to spatial scales. – Sci. Total Environ. **854**: 158743, 2023.

Houborg R., Fisher J.B., Skidmore A.K.: Advances in remote sensing of vegetation function and traits. – J. Appl. Earth Obs. Geoinf. **43**: 1-6, 2015.

IUSS Working Group WRB: World Reference Base for Soil Resources 2014. International Soil Classification System for Naming Soils and Creating Legends for Soil Maps. World Soil Resources Reports No. 106. Pp. 203. FAO, Rome 2015. *Available at*: https://openknowledge.fao.org/handle/20.500.14283/i3794en.

Kior A., Yudina L., Zolin Y. *et al.*: RGB imaging as a tool for remote sensing of characteristics of terrestrial plants: a review. – Plants-Basel **13**: 1262, 2024.

Lichtenthaler H.K., Babani F.: Contents of photosynthetic pigments and ratios of chlorophyll *a*/*b* and chlorophylls to carotenoids (*a*+*b*)/(*x*+*c*) in C_4 plants as compared to C_3 plants. – Photosynthetica **60**: 3-9, 2022.

López González G.A.: [The Trees and Shrubs of the Iberian Peninsula and the Balearic Islands.] 2nd Edition. 2 Volumes. Pp. 1731. Ediciones Mundi-Prensa, Madrid 2006. [In Spanish]

Lozanovska I., Bejarano M.D., Martins M.J. *et al.*: The functional diversity of riparian woody vegetation is less affected by river regulation in the Mediterranean than in the boreal region. – Front. Plant Sci. **11**: 857, 2020.

Mackinney G.: Absorption of light by chlorophyll solutions. – J. Biol. Chem. **140**: 315-322, 1941.

Martínez-Fernández V., Van Oorschot M., De Smit J. *et al.*: Modelling feedbacks between geomorphological and riparian vegetation responses under climate change in a Mediterranean context. – Earth Surf. Proc. Land. **43**: 1825-1835, 2018.

Milne B.F., Toker Y., Rubio A., Nielsen S.B.: Unraveling the intrinsic color of chlorophyll. – Angew. Chem. Int. Ed. **54**: 2170-2173, 2015.

Montes C., Llorca A., Sterling A.: [Guidelines for the Ecological Recovery of the Middle Section of the Manzanares River.] 1st Edition. Pp. 139. Canal de Isabel II, Madrid 1987. [In Spanish]

Mulero G., Bacher H., Kleiner U. *et al.*: Spectral estimation of *in vivo* wheat chlorophyll *a*/*b* ratio under contrasting water availabilities. – Remote Sens. **14**: 2585, 2022.

Newberry R.W., Raines R.T.: The n→ π* interaction. – Acc. Chem. Res. **50**: 1838-1846, 2017.

Pérez-Patricio M., Camas-Anzueto J.L., Sanchez-Alegría A. *et al.*: Optical method for estimating the chlorophyll contents in plant leaves. – Sensors **18**: 650, 2018.

Qiu N.W., Jiang D.C., Wang X.S. *et al.*: Advances in the members and biosynthesis of chlorophyll family. – Photosynthetica **57**: 974-984, 2019.

Regodón J.P.: [Geological, Hydrogeological, and Mining Guide of the Province of Madrid.] 1st Edition. Memorias del Instituto

Geológico y Minero de España, Madrid 1970. [In Spanish]
Riis T., Kelly-Quinn M., Aguiar F.C. *et al.*: Global overview of ecosystem services provided by riparian vegetation. – BioScience **70**: 501-514, 2020.
Ríos Cortés G.R.C., Ramírez Aguilar D., Bobadilla Reyes C.Q. *et al.*: Removal of chlorophylls present in stevia (*Stevia rebaudiana* Bertoni) extracts by activated carbon adsorption and precipitation with lime food grade. – Acta Univ. **27**: 67-75, 2017.
Rodríguez-González P.M., Stella J.C., Campelo F. *et al.*: Subsidy or stress? Tree structure and growth in wetland forests along a hydrological gradient in Southern Europe. – Forest Ecol. Manag. **259**: 2015-2025, 2010.
Sabo J.L., Sponseller R., Dixon M. *et al.*: Riparian areas increase regional species richness by harboring different species, not more species. – Ecology **86**: 56-62, 2005.
Santiago J.M., García de Jalón D.: Heat recovery as a tool for reducing the thermal impact of effluents from wastewater treatment plants. – Sustainability **18**: 3879, 2026.
Sinclair T., Craig P., Maltby L.L.: Climate warming shifts riverine macroinvertebrate communities to be more sensitive to chemical pollutants. – Glob. Change Biol. **30**: e17254, 2024.
Stella J.C., Bendix J.: Multiple stressors in riparian ecosystems. – In: Sabater S., Elosegi A., Ludwig R. (Eds.): Multiple Stressors in River Ecosystems: Status, Impacts and Prospects for the Future. Pp. 81-110. Elsevier, San Diego 2019.
Taniguchi M., Lindsey J.S.: Absorption and fluorescence spectral database of chlorophylls and analogues. – Photochem. Photobiol. **97**: 136-165, 2021.
Yan Z., Li P., Li Z. *et al.*: Dynamic response of soil enzyme activities in riparian zones: Insights from vegetation cover. – J. Soil Sci. Plant Nutr. **25**: 1597-1611, 2025.
Zahir S.A.D.M., Omar A.F., Jamlos M.F. *et al.*: A review of visible and near-infrared (Vis-NIR) spectroscopy application in plant stress detection. – Sensor. Actuat. A Phys. **338**: 113468, 2022.
Zahn C., Nag P., Stensitzki T. *et al.*: Orientation of the electronic Qy transition dipole moment in chlorophyll *a*. – J. Phys. Chem. B **130**: 5488-5494, 2026.

© The authors. This is an open access article distributed under the terms of the Creative Commons BY-NC-ND Licence.